Effects of curvature on the propagation of undulatory waves in lower dimensional elastic materials

Jonathan Kernes[1] and Alex J. Levine[1,2,3]
[1]*Department of Physics and Astronomy, UCLA, Los Angeles, California 90095-1596, USA*
[2]*Department of Chemistry and Biochemistry, UCLA, Los Angeles, California 90095-1596, USA*
[3]*Department of Computational Medicine, UCLA, Los Angeles, California 90095-1596, USA*

(Received 24 June 2020; accepted 16 December 2020; published 11 January 2021)

The mechanics of lower dimensional elastic structures depends strongly on the geometry of their stress-free state. Elastic deformations separate into in-plane stretching and lower energy out-of-plane bending deformations. For elastic structures with a curved stress-free state, these two elastic modes are coupled within linear elasticity. We investigate the effect of that curvature-induced coupling on wave propagation in lower dimensional elastic structures, focusing on the simplest example—a curved elastic rod in two dimensions. We focus only on the geometry-induced coupling between bending and longitudinal (in-plane) strain that is common to both rods in two dimensions and to elastic shells. We find that the dispersion relation of the waves becomes gapped in the presence of finite curvature; bending modes are absent below a frequency proportional to the curvature of the rod. By studying the scattering of undulatory waves off regions of uniform curvature, we find that undulatory waves with frequencies in the gap associated with the curved region tunnel through that curved region via conversion into compression waves. These results should be directly applicable to the spectrum and spatial distribution of phonon modes in a number of curved rod-like elastic solids, including carbon nanotubes and biopolymer filaments.

DOI: 10.1103/PhysRevE.103.013002

I. INTRODUCTION

Lower dimensional elastic structures are materials in which one (or more) of their characteristic length scales is small, while the others are not. Examples include biopolymer filaments [1] (two such small lengths and one large one), ribbons [2], and membranes or shells (one small length and two large ones) [3]. The physics of lower dimensional elastic structures is broadly applicable to problems ranging from nanometer lengths in carbon nanotubes [4,5] to $\approx 10^6$ meters when discussing continental plates [6]. In the purely biological context, lower dimensional elastic structures are central to several systems, including viral capsids [7–10] and cell membranes [11–13] as well as filaments and and their bundles.

Due to their having one (or more) small dimensions, lower dimensional elastic structures have a large separation of compliances typically separating the soft modes associated with bending normal to the small thickness direction and stiffer modes associated with deformations whose displacements lie normal to the small dimension directions. For example, a thin rod is typically easier to bend than it is to stretch [14]. This is also well known in the study of flat elastic plates, in which the out-of-plane motion of the sheet, that arises due to bending deformations, requires low energies when compared with in-plane deformations. For a shell of lateral extent L and thickness $h \ll L$, this separation of energy scales can be parametrized by the Föppl-von Kármán number $\nu K \sim (L/h)^2 \gg 1$ [15,16]. For a flat plate within linear elasticity theory, these soft bending modes decouple from the stiff in-plane deformations. When the elastic reference (stress-free) state of the shell is not flat, these modes are coupled by the local curvature. The result is that shells with complex geometry have significantly different elastic behavior [17–19]. For example, thin shells with local positive Gauss curvature in their stress-free state inhibit bending undulations [20]. Previous studies of the dynamics of undulatory waves on curved shells have shown that, in the geometric optics limit, these waves are reflected and refracted by changes in the local curvature. They can even undergo total internal reflection when propagating from regions of negative to positive Gaussian curvature [21]. Such effects have measurable implications for the spatial distribution of thermal undulations on red blood cells, which have regions of both positive and negative Gauss curvature [22].

The coupling of bending to stretching by curvature alters the normal-mode frequency spectrum by mixing in-plane and out-of-plane deformations. One may ask whether one could, in effect, "hear" the curvature of a shell by examining its eigenfrequencies of vibration. Famously, such a question was posed with regard to hearing the shape of a drum [23], which was in the negative [24]. We suggest by an example discussed below that one can, in fact, hear the shape of a bent rod; this has implications for understanding the phonon structure of some carbon nanotubes [25].

In this paper, we study the propagation of elastic waves on an undamped filament, where the elastic reference state couples bending and stretching deformations within the framework of linear elasticity. Our goal is go beyond the geometric optics analysis of undulatory waves and produce the analog of the Fresnel equations, allowing one to understand the transmission and reflection of elastic energy intensity at various geometric interfaces. The simplest model that retains

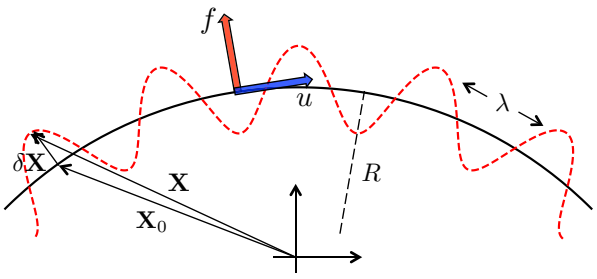

FIG. 1. Schematic representation of an undulatory wave on a curved rod. The (black) solid line is the space curve of the undeformed rod with radius of curvature R supporting a sinusoidal wave (not to scale) shown as the (red) dashed line. Deformations about the undeformed state are decomposed locally into a displacement u (wide blue arrow) along the local tangent, and a displacement f (wide red arrow) along the local normal. The weak-curvature approximation assumes that the radius of curvature R of the stress-free state (solid black line) is much larger than wavelength λ of characteristic deformations (dashed red line).

the geometric coupling of in-plane deformation and bending is the elastic rod. While we believe that these results will inform work on membranes with more complex curvature, the theory is directly applicable to a wide variety of filaments. After introducing the elastic Hamiltonian in Sec. II, we analyze in Sec. III the effect of uniform curvature on the eigenmodes of a rod, addressing the question of whether one can, in this instance, observe the effect of curvature on the mode spectrum. In Sec. IV, we look at the scattering of elastic waves on an infinite rod by localized regions of curvature, where we find that undulations can tunnel through curved regions that do not support such undulations in the bulk. Finally, we summarize our results and comment on their implications in Sec. V.

II. MODEL

We consider the elastic dynamics of a thin, curved rod embedded in two dimensions. We neglect twisting or torsional modes of deformation. Neglect of twisting can be justified by our treatment of the rod's cross section as infinitesimal. By neglecting this coupling, we focus on the geometric bend-stretch coupling that is common to both rods and elastic shells or membranes. We note that, for the case of shells in three dimensions, we may neglect torsion because it does not exist for surfaces of codimension one. A more detailed explanation is given following Eq. (5). We do not consider the elastic deformation of the material in the rod's cross section. Where applicable, we state the results for a rod of uniform cross section and composed of isotropic elastic continuum with uniform elastic constants.

We develop the mechanics of curved rods by determining the action from which the equations of motion are derived. We work in the weak-curvature limit shown schematically in Fig. 1. The weak-curvature limit is equivalent to the inequalities $h \ll \lambda \ll R$, where h represents the cross-sectional radius, λ is the length of characteristic deformations, and R is the local radius of curvature. This is a one-dimensional version of the linearized shallow shell theory approximations [15,21].

The stress-free configuration of the rod, shown in Fig. 1, is described by a two-dimensional space curve $\mathbf{X}_0(s)$, where s denotes the arclength. The local tangent is given by $\hat{\mathbf{t}} = d\mathbf{X}_0/ds$. One may also compute the local normal (and binormal, which is trivial for the rod embedded in the plane) vectors via the well-known Frenet-Serret relations [26]. We may write these relations as

$$\frac{d\hat{\mathbf{t}}}{ds} = \kappa(s)\hat{\mathbf{n}}, \quad \frac{d\hat{\mathbf{n}}}{ds} = -\kappa(s)\hat{\mathbf{t}}, \tag{1}$$

where $\kappa(s)$ is the arclength-dependent curvature [equivalent to the inverse radius of curvature $R(s)$], $\hat{\mathbf{n}}$ the local normal vector, and bold-face symbols refers to two-dimensional vectors.

We choose to neglect self-intersections of the rod primarily because these introduce nonlocal (in s) interactions, which cannot be addressed using this formalism. There are two ways to justify this. One may assume that the curvature is sufficiently weak and the rod's length is sufficiently short that the curvature of the elastic reference state does not generate self-intersections. Second, one might assume that the rod is vanishingly thin and that, even upon looping, it avoids self-collisions by being displaced by an infinitesimal amount in the third dimension. However, the extension to three dimensions is known to introduce torsional instabilities. We do not address these here. We expect these torsional effects to be small in the limit of infinitesimally thin rods and note that the extension of the problem to infinitely long rods simplifies the analysis of the dispersion relation of coupled bending or stretching modes on the rod, as shown below.

Having neglected such self-intersections, we observe that the rod's elastic energy density is determined solely by its local state of deformation.

For small deformations $\delta X(s)$, the space curve describing the deformed state is then

$$\mathbf{X}(s) = \mathbf{X}_0(s) + \delta\mathbf{X}(s). \tag{2}$$

Translational invariance demands that the elastic energy $\mathcal{U}$ be a function of $\frac{d\mathbf{X}_0}{ds}$, $\frac{d\mathbf{X}}{ds}$, and their derivatives. Given the curved stress-free state of the rod, we also require that $\mathcal{U}$ vanishes when $\mathbf{X} = \mathbf{X}_0$. We obtain the elastic energy

$$\mathcal{U} = \frac{1}{2}\int ds[aU^2 + bK^2], \tag{3}$$

where a and b represent phenomenological parameters. We have also introduced the one-dimensional longitudinal strain tensor

$$U = \frac{1}{\sqrt{2}}\left[\left|\frac{d\mathbf{X}}{ds}\right|^2 - \left|\frac{d\mathbf{X}_0}{ds}\right|^2\right]^{1/2} = \hat{\mathbf{t}}\cdot\frac{d\delta\mathbf{X}}{ds} + O(\delta X^2), \tag{4}$$

and the bending tensor

$$K = \frac{1}{\kappa\sqrt{2}}\left[\left|\frac{d^2\mathbf{X}}{ds^2}\right|^2 - \left|\frac{d^2\mathbf{X}_0}{ds^2}\right|^2\right]^{1/2} = \hat{\mathbf{n}}\cdot\frac{d\delta\mathbf{X}}{ds} + O(\delta X^2). \tag{5}$$

For the case in which the reference state is straight, these two contributions to the elastic Hamiltonian—see Eqs. (3)–(5)—reduce to the standard definition of longitudinal strain or stretching and out-of-plane bending. As a result, we refer to the first and second terms of Eq. (3) as *bending* and

stretching, respectively. Then, a and b have the interpretation of elastic constants. We define the stretching [Eq. (4)] and bending [Eq. (5)] strains, with square roots and squares in the energy functional in order to align with the generalized representation of elasticity in higher dimensions [10,15]. One can certainly derive the energy functional without introducing the squares and square roots—see Refs. [27,28]. As shown in these references, one obtains the correct geometric nonlinearities for the problem using that method. We do not explore these higher-order in $\delta\mathbf{X}$ corrections.

For rods (and generally for objects of codimension greater than one), there exist additional torsional degrees freedom that contribute to the elastic energy [29]. These consist of displacements normal to both the local tangent(s) as well as the unique bending normal orthonormal to the covariant derivative of a local geodesic. The generalized Serret-Frenet relations require that each additional normal vector be proportional to the $m > 1$ derivative of the local tangent with respect to arc length. For weakly curved rods, these torsional terms constructed out of higher-order derivatives may be neglected in comparison with the aforementioned bending and stretching contributions.

Deformations are parametrized in normal coordinates [3]

$$\delta\mathbf{X} = u\hat{\mathbf{t}} + f\hat{\mathbf{n}}, \tag{6}$$

where u represents a local in-plane displacement that leads to stretching deformations, and f represents local out-of-plane displacements that lead to bending. Rewriting U and K in terms of normal coordinates, we find (using primes to denote arc length derivatives)

$$U = u' - \kappa f, \tag{7}$$

and

$$K = f'' + 2\kappa u' + \kappa' u - \kappa^2 f. \tag{8}$$

In the weak-curvature limit, the second and fourth terms are negligible. The third term is more subtle. It can certainly be discarded for rods with constant curvature, which we study here, but also may be discarded provided R'/R is small. We thus find $K \approx f''$.

To determine the action, we introduce the kinetic energy, taking the mass density (mass per unit length) of the rod to be ρ. In the weak-curvature limit, the kinetic-energy density can be approximated by its flat rod result, as corrections are higher order in curvature. Using dots (primes) for time (spatial) derivatives, we obtain the action

$$S = \frac{1}{2}\int ds\{\rho\dot{f}^2 + \rho\dot{u}^2 - a(u' - \kappa f)^2 - bf''^2\}. \tag{9}$$

For a uniform elastic rod with Young's modulus Y, cross sectional area A, and moment of inertia I, the two phenomenological elastic constants can be expressed in terms of these more microscopic ones as $a = YA$ and $b = YI/2$ [14]. We may eliminate the dependence on a, b by a suitable rescaling of length and time, introducing dimensionless independent variables: $s \to s/\ell^*$ and $t \to t/t^*$, where

$$\ell^* = \sqrt{\frac{b}{a}}, \tag{10}$$

$$t^* = \frac{\sqrt{b\rho}}{a}. \tag{11}$$

Variations with respect to u and f yield the equations of motion

$$\partial_t^2 f + \partial_s^4 f + M^2 f = M\partial_s u, \tag{12a}$$

$$\partial_t^2 u - \partial_s^2 u = -\partial_s(Mf), \tag{12b}$$

where we have defined the dimensionless curvature

$$M(s) = \ell^*/R(s), \tag{13}$$

in terms of the arc length dependent stress-free radius of curvature $R(s)$. Equations (12a) and (12b) are one-dimensional versions of the linearized shallow shell equations governing thin shells [15].

The boundary conditions are also obtained by variation of the action. In addition to continuity of u, f, and f' across the boundary, we find three force balance equations. These equations require the continuity

$$\Delta(u' - Mf) = 0, \tag{14}$$

$$\Delta(f'') = 0, \tag{15}$$

$$\Delta(f''') = 0, \tag{16}$$

across an interface where the curvature of the rod changes, say at $s = 0$. In the above equations we use the notation $\Delta(\phi) = \lim_{s\to 0^+}\phi - \lim_{s\to 0^-}\phi$ to represent the discontinuity of some variable ϕ across a boundary. At a boundary where the curvature changes discontinuously, there is a subtlety in that κ' is not well defined, suggesting that we are not justified in discarding the term $\kappa' u$ in the bending tensor K—see Eq. (8). However, in the presence of discontinuous curvature, our assumptions leading to the derivation of K cease to hold as well. Physically, the boundary conditions (14)–(16) represent longitudinal force balance, transverse force balance, and torque balance across the interface, respectively. Within the linearized shallow shell theory [15] approximation $K \approx f''$, these boundary conditions still provide the correct physical continuity of force and torque. Equation (12) and boundary conditions (14)–(16) represent the minimal coupling of an elastic rod to curvature.

III. EIGENMODES AND FREQUENCIES

We consider the case of constant curvature, which corresponds to the replacement $M(s) \to M$. Equations (12a) and (12b) now constitute a set of linear partial differential equations. In the frequency domain, these equations can be made to appear like the time-independent Schrödinger equation for a spinor-valued state ket $|\psi\rangle$:

$$\hat{H}\,|\psi\rangle = \omega^2\,|\psi\rangle\,, \tag{17}$$

which may be written in the s or arclength basis

$$\langle s|\psi\rangle = f(s)\,|f\rangle + u(s)\,|u\rangle\,, \tag{18}$$

in terms of basis spinors $|f\rangle = (1\,0)^T$ and $|u\rangle = (0\,1)^T$, and two "wave functions" $f(s)$ and $u(s)$, which correspond to the amplitude of bending and stretching deformation, respectively. In terms of this spinor fu basis, the Hamiltonian is

given by

$$\hat{H} = \begin{pmatrix} \partial_s^4 + M^2 & -M\partial_s \\ M\partial_s & -\partial_s^2 \end{pmatrix}. \tag{19}$$

Note that the f and u problems decouple on a straight rod ($M = 0$) as expected—see below. We look for traveling-wave solutions of the form $e^{iks}|\psi_k\rangle$, where the spinor $|\psi_k\rangle$ is s-independent. The Hamiltonian acting on such a state becomes

$$\hat{H}(k, M) = \begin{pmatrix} k^4 + M^2 & -iMk \\ iMk & k^2 \end{pmatrix}. \tag{20}$$

A. Zero curvature

We briefly review the case of zero curvature ($M = 0$). The Hamiltonian is diagonal, with eigenfrequency and eigenstate pairs

$$(\omega = k) \leftrightarrow |u\rangle\,, \quad (\omega = k^2) \leftrightarrow |f\rangle\,. \tag{21}$$

f and u waves have quadratic and linear dispersion relations, respectively. In their mode spectrum there are three points of degeneracy: $k = 0, \pm 1$.

For a finite rod of length ℓ, boundary conditions restrict the allowed values of wave number k, producing a discrete spectrum of eigenvalues or frequencies. We consider a clamped rod, requiring that u, f, and f' vanish at the boundary. The eigenvalue equation [Eq. (17)] has a solution of the form $|\psi(s)\rangle = e^{iks}|\psi_k\rangle$, provided that $\det(\omega^2\mathbb{1} - \hat{H}(k)) = 0$. This is satisfied for any wave number k that fulfills the condition

$$(\omega^2 - k^2)(\omega^2 - k^4) = 0. \tag{22}$$

There are six solutions. These include two propagating u waves of the form $e^{\pm i\omega s}|u\rangle$, two propagating f waves of the form $e^{\pm i\sqrt{\omega}s}|f\rangle$, and two exponential (evanescent) f waves corresponding to imaginary solutions of wave number. These are given by $e^{\pm\sqrt{\omega}s}|f\rangle$.

We determine the allowed frequencies by first projecting $|\psi\rangle$ onto the wave number basis,

$$\psi(k) = \sum_{\sigma=\pm} c_\sigma^u e^{\sigma i\omega s}|u\rangle + \left(c_\sigma^f e^{\sigma i\sqrt{\omega}s} + c_\sigma^{E,f} e^{\sigma\sqrt{\omega}s}\right)|f\rangle\,, \tag{23}$$

in terms of the undetermined coefficients $c_\pm^u$, $c_\pm^f$, $c_\pm^{E,f}$. The six boundary conditions (three at each end) produce a set of six equations for the six coefficients. A solution exists provided the determinant of the coefficient matrix vanishes, yielding the eigenfrequency condition

$$[\cos(\sqrt{\omega}\ell)\cosh(\sqrt{\omega}\ell) - 1]\sin(\omega\ell) = 0. \tag{24}$$

Frequencies ω_f that cause the bracketed expression to vanish correspond to purely $|f\rangle$ bending modes, whereas frequencies ω_u that cause the sine to vanish are purely $|u\rangle$ stretching modes. Since the function $\cosh(x)$ grows exponentially with its argument, to good approximation, we may use the approximate f-mode frequency condition $\cos(\sqrt{\omega_f}\ell) = 0$ when $\sqrt{\omega}\ell > 1$. This leads to the (approximate) solutions for the bending-mode eigenfrequencies

$$\omega_f \approx \left(\frac{(n + 1/2)\pi}{\ell}\right)^2, \tag{25}$$

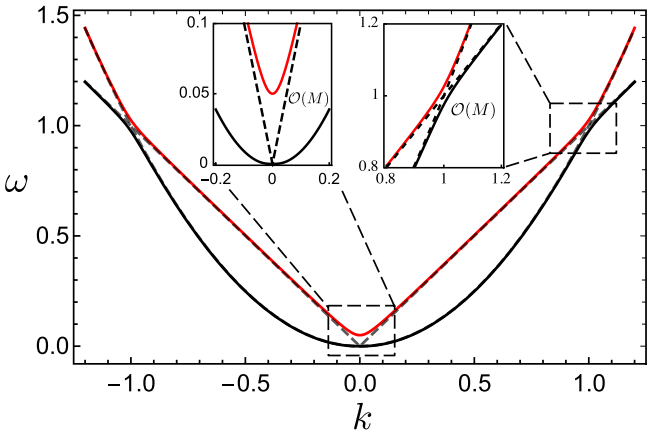

FIG. 2. Dispersion relation of a uniformly curved rod of infinite extent with $M = 0.05$. The degeneracy between the $M = 0$ dispersion curves (dashed black lines) is lifted due to curvature. Level splitting between the upper branch (red) and lower branch (black) is $O(M)$ near wave numbers $k = \pm 1$ and $k = 0$.

for positive integers n. The stretching eigenfrequencies, which correspond to vanishing of $\sin(\omega_u\ell)$, are easily found to be

$$\omega_u = \frac{n\pi}{\ell}. \tag{26}$$

B. Uniform curvature

In the presence of uniform curvature M, the eigenfrequencies of Eq. (20) split into two branches:

$$\omega_\pm^2 = \tfrac{1}{2}[(k^4 + k^2 + M^2) \pm \sqrt{(k^4 + k^2 + M^2)^2 - 4k^6}], \tag{27}$$

where the $(+)$ subscript refers to the upper branch, and the $(-)$ subscript to the lower. In the limit $M \to 0$ and $|k| > 1$, these reduce to $\omega_+ = k^2$ and $\omega_- = k$, indicating that the upper branch corresponds to a bending mode, and the lower branch to a stretching mode. For $|k| < 1$, the identification is reversed, with $\omega_+ = k$ and $\omega_- = k^2$. These identifications are further supported by looking at the (unnormalized) eigenmodes, which may be written as

$$|+\rangle = |f\rangle + \frac{-ikM}{k^2 - \omega_+^2(k, M)}|u\rangle\,, \tag{28}$$

$$|-\rangle = |u\rangle + \frac{ikM}{k^4 + M^2 - \omega_-^2(k, M)}|f\rangle\,. \tag{29}$$

For $|k| > 1$, the $M \to 0$ limit recovers the zero-curvature results $|+\rangle = |f\rangle$ and $|-\rangle = |u\rangle$. Again, the identifications are reversed for $|k| < 1$. For a rod of infinite length, the range of allowed k values is continuously infinite. For a finite-length rod, these modes become discrete with a countably infinite number of allowed values of k; these values depend on the details of the boundary conditions imposed at the ends of the rod.

In Fig. 2, we plot the dispersion relations of elastic waves on the rod at fixed $M \neq 0$. Curvature lifts the degeneracies at wave numbers $k = 0, \pm 1$. The magnitude of the level splitting is $O(M)$. The upper branch is gapped; it does not tend to zero with wave number, but instead to $\omega(k = 0) = M$. In this sense, the upper branch acts as if it has acquired a *mass*

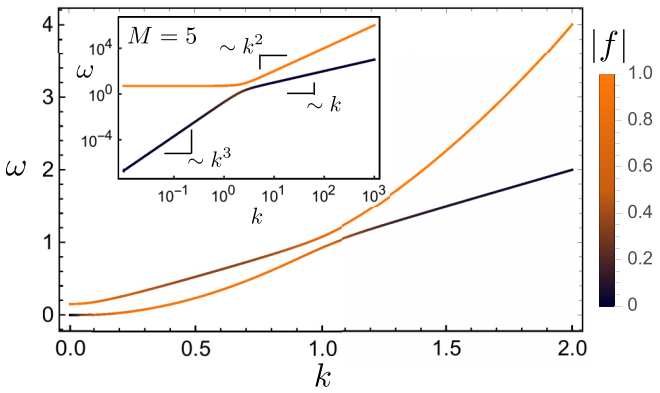

FIG. 3. The dispersion relation of a rod with uniform curvature, color-coded according to the normalized amplitude of its corresponding $|f\rangle$ eigenstate. $M = 0.15$ and $\ell = 1$. Mode mixing is strongest near the degeneracy points of the $M = 0$ case. In the inset, we show the behavior for larger curvature $M > 1$. At small k, the upper branch is essentially flat, while the lower branch develops an $\omega_- \approx |k|^3/M$ power law, in contrast to its quadratic dispersion relation at small curvature.

due to curvature, hence our use of the notation M. If the system possess frequencies $\omega < M$, they must have complex wave number and are necessarily bound. At finite M, in the limit $k \to 0$, the eigenmode of the upper branch becomes a pure $|f\rangle$ mode. Bending modes are gapped in the presence of curvature, which can be viewed as the one-dimensional analog of the suppression of undulations on thin shells at areas of positive Gauss curvature [20,21]. In the case of shells, this suppression is due to a change in character of the elasticity equations from hyperbolic to elliptic upon changing the sign of Gauss curvature [15]. Here, the effect manifests as a gap in the dispersion.

In the absence of curvature, the linear and quadratic dispersion corresponded to directly to $|u\rangle$ and $|f\rangle$ normal modes. In the presence of curvature, these normal modes are mixed. In Fig. 3, we show the same free dispersion relation color coded by normal-mode amplitude. The amplitudes obey the normalization constraint $|u|^2 + |f|^2 = 1$, which implies that $|f| = 1$ when $|u| = 0$, and vice versa. The effects of mode mixing are most prevalent at wave numbers near level splitting. At these points, the normal-mode amplitudes of the two branches switch character between u and f dominated. This ensures that only bending (stretching) dominated normal modes exhibit quadratic (linear) dispersion at large wave number. For wave number $k < 1$, the lower branch $\omega_- \sim |k|^3/M$, in contrast to the zero-curvature quadratic dispersion.

At fixed k, the frequencies on the upper (lower) branch of Eq. (27) increase (decrease) with increasing M. At large k, the frequencies on the lower branch decrease $\approx M^{-1}$, while those on the upper branch are hyperbolic and approach the asymptote $\omega = M$. As a result, frequencies ω_+ may never fall below M. This is due to the $k = 0$ band gap shown in Fig. 2 (see the inset of that figure).

The large-curvature limit of Eqs. (28) and (29) shows that the eigenstates that mix bending and stretching modes once again decouple so that $|+\rangle \to |f\rangle$ and $|-\rangle \to |u\rangle$. Interestingly, this is the same result as for $M \to 0$. Since at large M the $|+\rangle$ states become pure bending modes, we deduce that bending-dominated modes may not have frequencies $\omega < M$. Moreover, by increasing the curvature, one can identify which eigenfrequencies are related to primarily bending (stretching) dynamics, by seeing if they increase (decrease) with M. At larger curvature, due to the frequency gap, these frequencies are separated by the line $\omega = M$.

We now turn from the case of an infinite rod to a finite one. For a finite rod, we must impose boundary conditions at the ends, which generally lead to a quantized set of eigenfrequencies ω_n. To study how the frequency spectrum changes with respect to curvature, we fix clamped boundary conditions at the ends and vary only the curvature M. Thus, we demand that u, f, and f' vanish at the endpoints $s = 0,\ \ell$.

Following the steps of Sec. III A to determine the eigenfrequencies involves solving a cubic characteristic equation for k^2 as a function of ω, followed by finding the roots of an analytically complicated transcendental equation. Instead, we compute the eigenfrequencies and eigenfunctions directly in position space numerically, using collocation methods on a Chebyshev grid [30]. The eigenmode amplitudes are determined via numerical integration

$$\frac{\int_0^\ell |f|^2 ds}{\int_0^\ell (|f|^2 + |u|^2) ds},$$

performed via quadrature.

In the upper panel of Fig. 4, we plot the eigenfrequencies as a function of curvature for a rod of length $\ell = 20$, color coded so that an increasing ratio of bending to stretching amplitude runs from dark to light. Broadly speaking, frequencies that increase with respect to curvature are associated with bending f modes, and such modes are still restricted to frequencies $\omega > M$. The lower frequency modes show more mixing of bending and stretching.

Due to changing the rod's curvature, spectral lines (frequencies) corresponding to different modes cross. There are three regimes, dictated by the strength of interaction between different harmonics. At high frequency (and accordingly high $|k|$), curvature-induced coupling between bending and stretching is negligible. The spectral curves can be well approximated by using the zero-curvature k values, Eqs. (25) and (26), in the equations for the ω_+ and ω_- branches. As for the infinite rod, bending (stretching) modes increase (decrease) with increasing curvature. At low frequencies, curvature significantly affects the rod, and the free dispersion relation gives a poor fit.

At intermediate frequencies (approximately $1 < \omega < 1.75$ in the upper panel of Fig. 4), frequencies exhibit oscillatory behavior due to level splitting between other harmonics. To understand this effect, we expand the state $|\psi\rangle$ of Eq. (17) in the basis of zero-curvature eigenmodes

$$|\psi\rangle = \sum_n c_n(M) \left|\psi_n^{(0)}\right\rangle, \tag{30}$$

for some M-dependent coefficients. This leads to an equation for the coefficients c_n:

$$\left[\omega^2(M) - \omega_n^2\right] c_n = \sum_m \left\langle \psi_n^{(0)} \middle| \hat{V} \middle| \psi_m^{(0)} \right\rangle c_m, \tag{31}$$

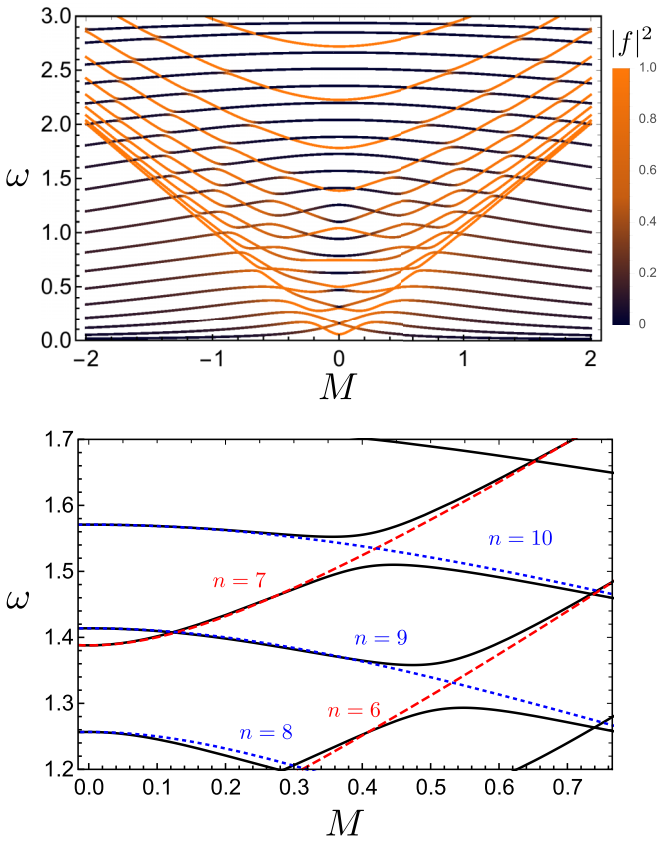

FIG. 4. The frequency spectrum of a clamped rod of length $\ell = 20$ as a function of curvature M. (top) The M-dependence of the frequency spectrum, color coded by the relative amplitude of its f to u mode, where lighter colors represent more bending f amplitude. Due to parametric M dependence, each curve represents one eigenmode. We find three distinct regimes: high ω where the curves look like their infinite-rod counterparts, intermediate ω, where the spectrum is approximated by free dispersion curves with level splitting, and low ω where curvature strongly distorts the spectrum. (bottom) a close up view of the frequency spectrum (black solid lines) overlaid with the infinite rod dispersion curves for several modes labeled by n in the figure (dashed lines). Level splitting occurs between even- and odd-numbered modes, as explained in the text.

where we have introduced the $M = 0$ eigenfrequencies ω_n corresponding to the eigenmodes $|\psi_n\rangle$, and we have defined the perturbation operator

$$\hat{V} = \begin{pmatrix} M^2 & -M\partial_s \\ M\partial_s & 0 \end{pmatrix}. \tag{32}$$

The perturbed eigenfrequencies $\omega(M)$ retain implicit dependence on the curvature M. For the infinite rod, the direct solution of Eq. (30) leads to the frequencies and states $\omega_\pm$, $|\pm\rangle$. We do not try to recover this result, but instead look at the possible straight-rod states coupled by the perturbation operator. Evaluating the off-diagonal matrix elements of V_{mn} we find

$$\langle m|\hat{V}|n\rangle_{m\neq n} = -2M \int_0^\ell f_m \partial_s u_n ds, \tag{33}$$

where f_m and u_m represent the zero-curvature eigenfunctions corresponding to the mth and nth eigenfrequencies—see Eqs. (25) and (26). The zero-curvature Hamiltonian $\hat{H}_0$ is invariant under a parity transformation $\hat{H}_0(s) = \hat{H}_0(-s)$. As a result, the eigenfunctions f_n and u_n are either even or odd. Since the operator ∂_s is odd under parity, the operator $\hat{V}$ connects states of opposite parity. The coupling $V_{m\neq n}$ is nonvanishing only when m is even and n is odd, or vice versa. In the lower panel of Fig. 4, we show a close-up view of the frequency spectrum overlaid with the free dispersion curves shown as dashed red (bending) and blue (stretching) lines. These lines are labeled by their mode number n shown in the corresponding color above each line in the figure. One observes level splitting and repulsion between odd and even harmonics, which leads to the oscillatory-like behavior. The level repulsion observed at, e.g., $M = 0.4$ and $\omega = 1.55$ is well known in quantum mechanics [31]. We point out that the small-ω modes at higher M have a sufficiently long wavelength (small k) that they violate the weak-curvature approximation that the wavelength of the modes be smaller than the local radius of curvature: $\lambda < 1/R$.

IV. SCATTERING

We study the transmission and reflection of undulatory and compression waves through regions of nonzero curvature. We imagine the scattering problem as follows: Two semi-infinite straight rod segments are appended to the left and right sides of a region of constant curvature M (i.e., the arc of a circle), such that both the rod and its tangents are everywhere continuous. We choose a coordinate system so that the center $s = 0$ is the symmetry point of the figure and note that the circular arc has length ℓ. The curvature jumps discontinuously from $0 \to M$ on the left, and $M \to 0$ on the right. See Fig. 5.

In the straight domains $|s| > \ell/2$, waves are defined by the eigenmodes and eigenfrequencies of Sec. III A. Radiative incoming and outgoing states are thus determined solely by the basis of plane-wave solutions, i.e., values of k that satisfy the infinite-rod dispersion relation. After demanding that the solution be finite at $\pm\infty$, each semi-infinite rod has five such solutions: an incoming and outgoing f wave, an incoming and outgoing u wave, and one evanescent f wave.

In the curved domain $s \in [-\ell/2,\ \ell/2]$, k can take complex values. This differs from the well-known transmission through a barrier in quantum mechanics, where the allowed k values are either purely real or imaginary [31]. In general, states with real k correspond to propagating solutions and facilitate transmission. We refer to the number of propagating solutions in the curved region as the number of *channels*, whereby a wave may be transmitted through the curved domain. Before computing transmission or reflection coefficients for an incoming plane wave, we study how the number of available channels is set by the combination of both the curvature of the rod and the frequency of an incoming plane wave.

The characteristic equation is found by demanding that the eigenvalue problem defined by Eq. (17) with the Hamiltonian given by Eq. (20) has a solution. This is ensured provided

$$\det[\omega^2 \mathbb{1} - \hat{H}(k, M)] = 0. \tag{34}$$

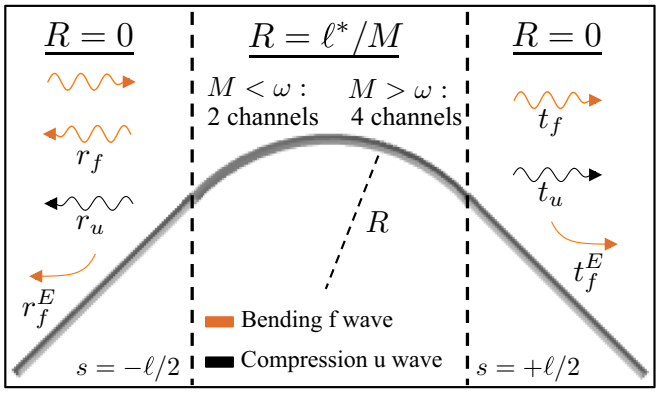

FIG. 5. Schematic representation of an elastic rod (solid gray line) formed by adjoining two semi-infinite straight rods at the (black) dashed lines to the left ($s = -\ell/2$) and right ($s = \ell/2$) of the curved rod segment (arc of a circle with radius R), such that the rod and its tangent are everywhere continuous. We consider the scattering of an incoming bending f wave from the left, through the region of constant curvature M. Curvy arrows correspond to propagating asymptotic states, and decaying arrows to evanescent states. The darker (lighter) colors refer to u (f) modes. There are six unknown transmission and reflection amplitudes. In the curved region, there are either two or four propagating channels, determined by the value of M.

We find that the characteristic equation for $\kappa = k^2$ is cubic:

$$\kappa^3 - \omega^2\kappa^2 - \omega^2\kappa - \omega^2(M^2 - \omega^2) = 0. \tag{35}$$

Real solutions $\kappa < 0$ and $\kappa > 0$ correspond to evanescent and propagating waves, respectively. Complex κ corresponds to damped propagating waves.

The number of channels is twice the number of real, positive roots κ. These roots are a function of frequency and curvature. At zero curvature ($M = 0$), there are three roots at $\kappa = \pm\omega, \kappa = \omega^2$, leading to four channels (two pure f waves, and two pure u waves). At nonzero M, Descartes' rule of signs states that the number of positive (negative) roots is equal to or less than (by an even number) the number of sign changes of the coefficients when ordered in decreasing powers of κ ($-\kappa$).

For $M > \omega$, the polynomial coefficients undergo one sign change. There is only one positive root. When $0 \leqslant M < \omega$, Descartes' rule determines that there are either two or zero positive roots. In the limit $M = 0$, we already know that the characteristic equation contains two positive roots, and has a positive y intercept. Increasing M will only serve to shift the characteristic polynomial downward, while keeping the y intercept positive for $0 \leqslant M < \omega$. This shift cannot remove the two positive roots. We conclude that for $0 \leqslant M < \omega$ the characteristic polynomial has two positive roots.

In summary, there are four available channels when $0 \leqslant M < \omega$, but for $M > \omega$ there are only two available channels. The reduction in the number of channels with decreasing frequency can be traced back to the vanishing of f-dominated eigenmodes for frequencies $\omega < M$. However, the two available channels are not pure u modes but instead some combination of f and u displacements. This mixing of the modes allows pure f or u modes to interconvert in the presence of curvature, which has implications for phonon transmission through curved regions.

Transmission and reflection through constant curvature

We consider the case of an incoming, purely f-mode wave $e^{i\sqrt{\omega}s}\,|f\rangle$, or a purely u-mode wave $e^{i\omega s}\,|u\rangle$. In both cases, we take the incident wave to have unit amplitude far to the left of the circular arc. The wave, scattered by the curved region, produces two transmitted f and u waves with transmission amplitudes t_f and t_u, two reflected waves with amplitudes r_f and r_u, and two evanescent waves with amplitudes r_f^E and t_f^E, which decay exponentially away from $s = \pm\ell/2$. The situation is summarized in Fig. 5.

The transmission (reflection) coefficient, denoted by a capital letter T (R), is defined as the ratio of the outgoing flux of amplitude to the incoming flux. The flux is given by the product of the amplitude squared times the group velocity. For an incoming f wave of unit amplitude, the f-mode transmission and reflection coefficients are

$$T_f = |t_f|^2, \quad R_f = |r_f|^2. \tag{36}$$

However, since bending and compression waves obey different dispersion relations, we must account for their difference in group velocity. Compression u waves have unit velocity, while bending waves have a group velocity of $d\omega/dk = 2\sqrt{\omega}$. For an incoming f wave, the transmitted and reflected u waves are given by

$$T_u = \frac{|t_u|^2}{2\sqrt{\omega}}, \quad R_u = \frac{|r_u|^2}{2\sqrt{\omega}}. \tag{37}$$

To solve for the transmission and reflection coefficients, we must explicitly solve Eq. (17) at nonzero M and then employ the boundary conditions—(14)–(16)—to stitch together solutions at the boundaries $s = \pm\ell/2$.

Since we are looking for plane-wave solutions of the form $|\psi(s)\rangle = e^{iks}\,|\psi_k\rangle$, we shall reformulate Eq. (17) as an eigenvalue problem of the operator ∂_s at fixed ω. This is accomplished by reducing all higher-order derivatives ∂_s through the introduction of new fields $f_a \equiv \partial_s^a f$ and $u_a = \partial_s^a u$, for integers $a \geqslant 0$. The resulting system of equations may be written as a vector differential equation

$$\partial_x\,|\chi\rangle = \hat{A}\,|\chi\rangle \tag{38}$$

for the six-dimensional vector

$$|\chi\rangle = \begin{pmatrix} u_0 \\ u_1 \\ f_0 \\ f_1 \\ f_2 \\ f_3 \end{pmatrix} \tag{39}$$

and matrix

$$\hat{A} = \begin{pmatrix} 0 & 1 & 0 & 0 & 0 & 0 \\ -\omega^2 & 0 & 0 & M & 0 & 0 \\ 0 & 0 & 0 & 1 & 0 & 0 \\ 0 & 0 & 0 & 0 & 1 & 0 \\ 0 & 0 & 0 & 0 & 0 & 1 \\ 0 & M & \omega^2 - M^2 & 0 & 0 & 0 \end{pmatrix}. \tag{40}$$

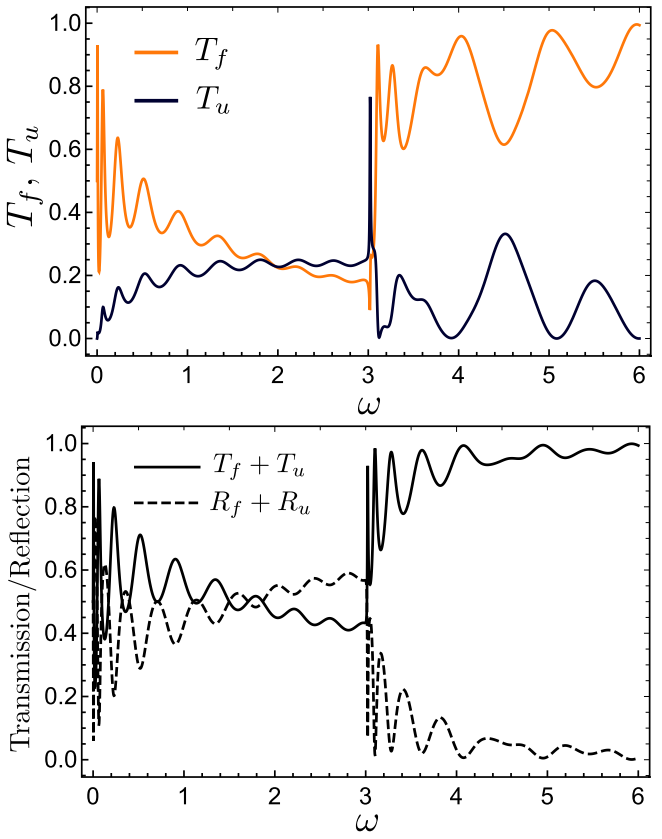

FIG. 6. Transmission and reflection coefficients for a bending wave of unit amplitude incident on a region of length $\ell = 10$, with uniform curvature $M = 3$. (top) The transmission coefficients for bending (orange) and compression (black) waves. (bottom) The total transmission and reflection coefficients. Due to conservation of energy, the coefficients obey $T_f + T_u + R_f + R_u = 1$. Curvature mixes eigenmodes, converting the incident pure bending wave into a linear combination of bending and compression waves.

The boundary conditions are now algebraic relations among all these fields. For a trial solution of the form $e^{iks}|\chi_k\rangle$, there are six possible solutions in the curved region, one for each value k that is a root of the characteristic polynomial—see Eq. (35). The full solution is given by a linear superposition of these trial solutions with six undetermined coefficients. We also have six more undetermined coefficients associated with the incident, reflected, and transmitted waves, giving a total of twelve undetermined coefficients. These are fixed by imposing the continuity of u, f, and f' at $s = \pm\ell/2$ (six conditions), as well as the three force balance conditions—Eq. (14)—at $s = \pm\ell/2$ (six conditions). Thus, we have a system of twelve linear equations that can be solved for the scattering amplitudes.

We solve these equations numerically. In Fig. 6, we plot the transmission and reflection coefficients for an f wave of unit amplitude incident on an interval of length $\ell = 10$, with uniform curvature $M = 3$. In the upper panel of Fig. 6, we show both the bending and compression transmission coefficients separately. Due to conservation of energy, we can define a total transmission coefficient $T_{\rm tot} = T_f + T_u$ and reflection coefficient $R_{\rm tot} = R_f + R_u$ such that their sum $T_{\rm tot} + R_{\rm tot} = 1$ is unity. Although we consider only an incoming bending wave, we find that curvature allows the rod to convert bending into stretching deformations, leading to the production of compression waves.

At low frequencies, $\omega < M$, the circular arc of the rod cannot support bending-dominant modes. The nonzero transmission coefficient for incident bending waves indicates that the f waves can, in effect, tunnel through the curved region via conversion to compression u waves, which then convert back into outgoing bending f waves in the righthand straight segment of the rod. In the curved domain, the incoming bending mode propagates through one of the two available channels. As frequency increases through $\omega = M$, the number of available channels in the curved domain jumps from two to four. This leads to a dramatic increase in the transmission coefficient.

For higher frequencies $\omega > M$, the circular arc can support bending-dominant modes. As a result, the transmission coefficient for f waves in the upper panel of Fig. 6 is much larger than that for u waves and tends to one as $\omega \to \infty$. The two principal effects of curvature—conversion from bending to compression and suppression of bending modes—diminish at high frequency.

In addition to these jumps, the transmission coefficients are oscillatory. It is well known that peaks in the scattering amplitude correspond to bound states under a change of sign of the eigenvalue $\omega^2 \to -\omega^2$ [32]. Since f has these peaks, they must correspond to eigenmodes in the curved region, which we know to be u dominant. Therefore, the incident bending wave uses these u-dominant modes to "tunnel" through the curved region.

When $\omega < M$, the upper panel of Fig. 6 shows T_f and T_u oscillating in phase. This supports idea that bending modes propagate via compression-dominated eigenmodes in the curved domain. Alternatively, for $\omega > M$, T_f and T_u oscillate out of phase. Peaks in T_f occur at frequencies corresponding to bending-dominated bound states. The fact that T_f and T_u are now out of phase shows that bending f waves are not traversing the curved region by conversion into compression u waves.

Finally, we observe that T_f is a decreasing function of frequency in the domain $0 \leqslant \omega < M$, while T_u is an increasing function of frequency on that same domain. Transmission of bending waves is a minimum for frequencies just below $\omega = M$. This suggests that bending waves are most effective at tunneling through curvature for both small and large frequencies.

In Fig. 7 we show the transmission and reflection coefficients for the case of an incoming u wave. We find similar results. The main difference lies at frequencies $\omega < M$. Bending waves arise only if they are produced via mode coupling in the curved domain. We find that T_f follows T_u, decreasing as frequency goes to zero, in contrast to its behavior for a purely bending incoming wave.

V. CONCLUSION

We investigate the interplay of bending and stretching in a curved, one-dimensional elastic rod. This is the simplest model that retains both bending and stretching deformations

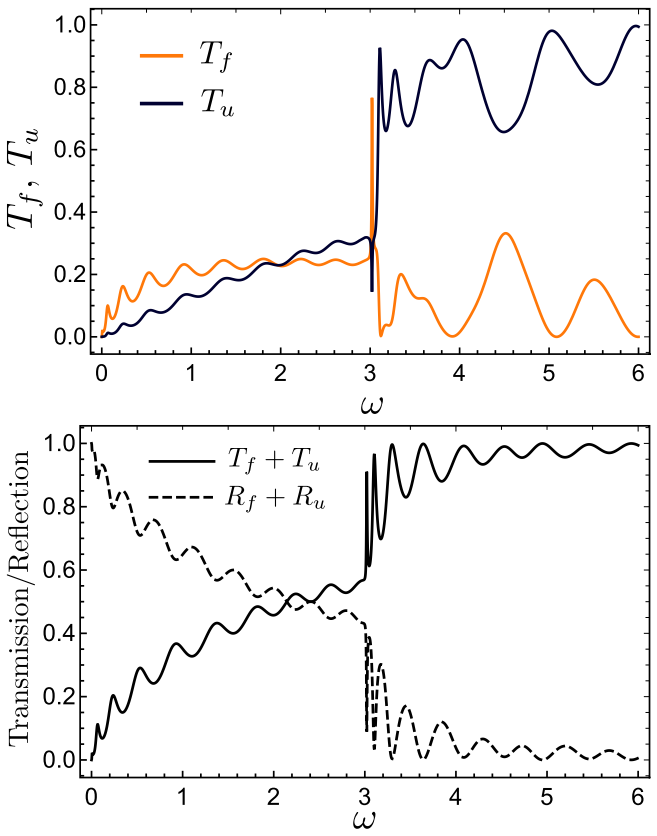

FIG. 7. Transmission and reflection coefficients for a compression wave of unit amplitude incident on a region of length $\ell = 10$, with uniform curvature $M = 3$. (top) The transmission coefficients for bending (orange) and compression (black) waves. (bottom) The total transmission and reflection coefficients. In contrast to an incident bending wave, see Fig. 6, the transmission coefficients vanish as $\omega \to 0$.

and allows their coupling via the geometry of the unstressed state [33]. In the limit of small deformations, we find a set of two coupled equations for out-of-plane deformations f and in-plane deformations u, corresponding to bending and stretching, respectively. These equations are the one-dimensional analog of the linearized shallow shell equations for a thin elastic shell. In fact, those equations reduce to the ones we study here in the limit of a membrane in which spatial variations occur along one direction only.

We find that there are two principal effects of curvature. The first is the opening of a frequency gap in the dispersion relation. This prevents bending f modes with frequencies $\omega < M$, with ω and M being the dimensionless frequency and curvature, respectively. This is the simpler one-dimensional equivalent of the suppression of bending undulations on membranes at areas of positive Gauss curvature [20,21]. For a finite rod with a discrete frequency spectrum, the restriction of $\omega > M$ for bending eigenfrequencies causes eigenfrequencies to cross with increasing curvature. By slowly bending a ringing rod, one can, in effect, "hear" the effects of curvature by noting that the modes split into an upper branch tending to the curve $\omega = M$ and a lower branch tending to zero. In this restricted sense, one can indeed hear changing curvature in a rod. We also note that one observes an oscillation of eigenfrequencies with respect to M as a consequence of level splitting among harmonics.

The second principal effect of curvature is the ability for undulatory f waves with frequency ω to tunnel through regions of curvature $M > \omega$. Although the curved region cannot support such bending waves, by coupling to in-plane modes, these undulatory waves can convert to compression waves in order to tunnel through curvature. This tunneling effect may be significant for understanding the propagation of flexural (bending) phonons over large distances in rods or membranes with complex curvature in their stress-free state. Physical examples should include the propagation of phonons in bent carbon nanotubes or ribbons. For the case of nanotubes, there are more elastic modes, such as radial "breathing" oscillations and torsion, which we do not address here. However, the basic coupling between bending and stretching imposed by the curvature of the elastic reference state will still apply to this more complex system. Finally, we note that the same geometrically induced coupling should affect the propagation of membrane undulations along cell membranes [22].

Open questions include how constitutive nonlinearities of the rod [34] which also cause flexural and longitudinal wave mixing interact with the geometric effects explored here. Additionally, one may inquire about rods with internal structures that lead to twist-stretch coupling, as is well known for DNA [35]. Finally, one may ask if multiple scattering of bending waves from randomly curved surfaces can lead to localization, and then consider how the "tunneling" of bending waves may affect this result.

ACKNOWLEDGMENTS

The authors thank Louis Foucard and Alexander Serov for fruitful discussions. This work was supported in part by NSF-DMR-1709785.

[1] C. P. Broedersz and F. C. MacKintosh, Rev. Mod. Phys. **86**, 995 (2014).
[2] A. Košmrlj and D. R. Nelson, Phys. Rev. B **93**, 125431 (2016).
[3] D. R. Nelson, T. Piran, and S. Weinberg, *Statistical Mechanics of Membranes and Surfaces*, 2nd ed. (World Scientific, Singapore, 2004).
[4] L. Wang and H. Hu, Phys. Rev. B **71**, 195412 (2005).
[5] C. Bower, R. Rosen, L. Jin, J. Han, and O. Zhou, Appl. Phys. Lett. **74**, 3317 (1999).
[6] P. Kearey, K. A. Klepeis, and F. J. Vine, *Global Tectonics*, 3rd ed. (John Wiley & Sons, Singapore, 2009).
[7] J. Lidmar, L. Mirny, and D. R. Nelson, Phys. Rev. E **68**, 051910 (2003).
[8] J. Michel, I. Ivanovska, M. Gibbons, W. Klug, C. Knobler, G. Wuite, and C. Schmidt, Proc. Natl. Acad. Sci. USA **103**, 6184 (2006).
[9] W. S. Klug, R. F. Bruinsma, J.-P. Michel, C. M. Knobler, I. L. Ivanovska, C. F. Schmidt, and G. J. L. Wuite, Phys. Rev. Lett. **97**, 228101 (2006).

[10] A. R. Singh, A. Košmrlj, and R. Bruinsma, Phys. Rev. Lett. **124**, 158101 (2020).
[11] R. Waugh and E. Evans, Biophys. J. **26**, 115 (1979).
[12] Y. Park, C. A. Best, K. Badizadegan, R. R. Dasari, M. S. Feld, T. Kuriabova, M. L. Henle, A. J. Levine, and G. Popescu, Proc. Natl. Acad. Sci. USA **107**, 6731 (2010).
[13] Y. Park, C. A. Best, T. Kuriabova, M. L. Henle, M. S. Feld, A. J. Levine, and G. Popescu, Phys. Rev. E **83**, 051925 (2011).
[14] L. Landau and E. Lifshitz, *Theory of Elasticity*, 3rd ed. (Pergamon, Oxford, 1986).
[15] F. Niordson, *Shell Theory* (North-Holland, Amsterdam, 1985).
[16] J. L. Sanders, Jr., Q. Appl. Math. **21**, 21 (1963).
[17] A. Lazarus, H. C. B. Florijn, and P. M. Reis, Phys. Rev. Lett. **109**, 144301 (2012).
[18] N. P. Bende, A. A. Evans, S. Innes-Gold, L. A. Marin, I. Cohen, R. C. Hayward, and C. D. Santangelo, Proc. Natl. Acad. Sci. USA **112**, 11175 (2015).
[19] A. Košmrlj and D. R. Nelson, Phys. Rev. E **88**, 012136 (2013).
[20] A. Vaziri and L. Mahadevan, Proc. Natl. Acad. Sci. USA **105**, 7913 (2008).
[21] A. A. Evans and A. J. Levine, Phys. Rev. Lett. **111**, 038101 (2013).
[22] A. A. Evans, B. Bhaduri, G. Popescu, and A. J. Levine, Proc. Natl. Acad. Sci. USA **114**, 2865 (2017).
[23] M. Kac, Am. Math. Mon. **73**, 1 (1966).
[24] C. Gordon, D. Webb, and S. Wolpert, Invent. Math. **110**, 1 (1992).
[25] A. W. Barnard, M. Zhang, G. S. Wiederhecker, M. Lipson, and P. L. McEuen, Nature (London) **566**, 89 (2019).
[26] M. D. Spivak, *A Comprehensive Introduction to Differential Geometry*, 3rd ed. (Publish or Perish, Houston, 1999).
[27] E. H. Dill, Arch. Hist. Exact Sci. **44**, 1 (1992).
[28] S. Lafortune, A. Goriely, and M. Tabor, Nonlinear Dyn. **43**, 173 (2006).
[29] B. D. Coleman, E. H. Dill, and D. Swigon, Arch. Ration. Mech. Anal. **129**, 147 (1995).
[30] L. N. Trefethen, *Spectral Methods in MATLAB* (SIAM, Philadelphia, 2000), Vol. 10.
[31] J. J. Sakurai and E. D. Commins, *Modern Quantum Mechanics, Revised Edition* (American Association of Physics Teachers, 1995).
[32] K. Gottfried and T.-M. Yan, *Quantum Mechanics: Fundamentals* (Springer Science & Business Media, 2013).
[33] A. E. Armenàkas, D. C. Gazis, and G. Herrmann, *Free Vibrations of Circular Cylindrical Shells* (Pergamon, 1969).
[34] A. Srivastava and F. L. di Scalea, J. Sound Vib. **329**, 1499 (2010).
[35] R. D. Kamien, T. C. Lubensky, P. Nelson, and C. S. O'Hern, Europhys. Lett. **38**, 237 (1997).